Optics & Laser Technology 58 (2014) 166–171

Contents lists available at ScienceDirect

Optics & Laser Technology

journal homepage: www.elsevier.com/locate/optlastec

# Comparative study of diode-pumped hydrocarbon free Rb and K vapor lasers

Fei Gao [a,b,*], Fei Chen [a], Jijiang Xie [a], Dianjun Li [a], Jingjiang Xie [a], Guilong Yang [a], Changbin Zheng [a], Yan Xu [a,b], Jin Guo [a]

[a] State Key Laboratory of Laser Interaction with Matter, Changchun Institute of Optics, Fine Mechanics and Physics, Chinese Academy of Sciences, Dong Nanhu Road 3888, Changchun 130033, Jilin, China
[b] University of Chinese Academy of Sciences, No. 19A Yuquan Road, Beijing 100039, China

ARTICLE INFO

*Article history:*
Received 11 October 2013
Received in revised form
18 November 2013
Accepted 21 November 2013
Available online 10 December 2013

*Keywords:*
Diode-pumped alkali vapor laser
Hydrocarbon free
Kinetic model

ABSTRACT

Based on the kinetic model of diode-pumped alkali vapor lasers, operation parameters including helium pressure, temperature and output mirror reflectivity are optimized for hydrocarbon free Rb laser and K laser. A comparative study on the output characteristics of hydrocarbon free Rb laser and K laser is also carried out. Results show that a better capability is presented in hydrocarbon free K laser instead of hydrocarbon free Rb laser, such as lower pump threshold, higher laser gain and optical-to-optical efficiency. The performance difference between K and Rb laser is mainly induced by the difference of helium pressure, which results in an evident difference on the absorption cross section and emission cross section.



## 1. Introduction

Diode-pumped alkali vapor lasers (DPALs) are three-level lasers emitting at near-infrared wavelengths (894.6 nm, 795.0 nm and 770.1 nm for Cs, Rb and K, respectively). They use vaporized alkali metal as gain medium, which should be simultaneously buffered by some gases like helium, ethane or methane. As gain mediums, alkali atoms have many intrinsic merits such as high quantum efficiency, large optical cross section, no stress birefringence, no stress fracture and low refraction index fluctuation, etc. Therefore, DPALs can be promising approaches for obtaining high efficiency, high output power and good beam quality near-infrared lasers. Thereby, DPALs have potential applications in many fields such as fundamental physical research, medical treatment, laser processing, etc. Especially, DPALs have the most promising applications in aerospace field for the laser wavelengths lie in the atmospheric window and have a good match with the absorption wavelengths of PV cells. Thus, diode-pumped alkali vapor lasers can be an ideal source for energy transfer from ground to PV cells mounted on satellites or space stations.

Since the first demonstration of Rb laser pumped by a surrogate Ti:Sapphire laser in 2003 [1], DPALs have been investigated extensively by many research groups during the last decade. The first Cs DPAL was reported in 2005 by Ehrenreich [2]. In these researches, many DPALs were operated in hydrocarbon buffer gas system, in which hydrocarbon gas like ethane or methane was used [3–5]. The results showed that Cs DPAL was more potential to generate high efficiency, high power laser output. The highest output power about 1 kW with optical-to-optical efficiency of 48% was demonstrated for Cs DPAL in 2012 [3]. But the output power for Rb laser or K laser was not so high as that of Cs laser [4,5]. Some theoretical work compared the laser performance between the three kinds of DPALs [6–8]. Especially based on the model by Yang [9], Wang investigated the efficiency of three kinds of DPALs. It was concluded that Cs DPAL had a higher efficiency due to its lower laser threshold, sufficient pump absorption and effective fluorescence suppression [8]. However, above experimental results and theoretical investigation were fundamentally based on the condition of no alkali-hydrocarbon reaction under high temperature. Actually, the reaction productions (alkali hydrate and carbon) will reduce the system lifetime of DPALs seriously. It was indicated that alkali hydrate and carbon would contaminate the cell windows when the local temperature was beyond 120 °C in Cs vapor cell [10]. To avoid alkali-hydrocarbon reaction, hydrocarbon free DPALs can be effective approaches. Hydrocarbon free DPALs use pure helium as buffer gas to achieve both the purposes of pressure-broadening and spin-mixing. Thus, the chemical reaction is naturally avoided. Due to the extremely small fine-structure mixing cross-section of Cs–He [11], hydrocarbon free DPALs can only be realized in Rb and K. The first hydrocarbon free Rb laser

* Corresponding author at: State Key Laboratory of Laser Interaction with Matter, Changchun Institute of Optics, Fine Mechanics and Physics, Chinese Academy of Sciences, Dong Nanhu Road 3888, Changchun 130033, Jilin, China.
Tel.: +86 431 86176196.
*E-mail address:* gaofei0104@163.com (F. Gao).

0030-3992/$ - see front matter 
http://dx.doi.org/10.1016/j.optlastec.2013.11.016

pumped by Ti:Sapphire laser was reported in 2007 with output power of 130 mW and optical-to-optical efficiency of 7% [12]. Output power of 28 W with an efficiency of 2% has been realized in hydrocarbon free Rb DPAL [13]. Moreover, overall efficiency of 57% has also been demonstrated in hydrocarbon free K laser with a pump source of alexandrite laser [14]. Thus, hydrocarbon free DPALs can be high efficiency laser systems for the aim of improving the system lifetime and stability.

In this paper, a kinetic model of end-pumped DPAL is carried out and the performance of hydrocarbon free Rb and K lasers is simulated for finding the optimal operation conditions. Due to the large difference in the cross section of spin-orbit energy exchange between Rb–He and K–He, helium pressure is considered as a main optimized parameter together with temperature and output mirror reflectivity. A comparative study between hydrocarbon free Rb and K lasers is investigated, and the results indicate that hydrocarbon free K laser has a higher laser gain and lower threshold pump power than that of Rb laser.

## 2. Kinetic model of alkali vapor lasers

As shown in Fig. 1, the pump and laser transitions of alkali atoms are realized in D2 line ($^2S_{1/2}\rightarrow{}^2P_{3/2}$) and D1 line ($^2P_{1/2}\rightarrow{}^2S_{1/2}$), respectively. The transition of excited population between fine structure levels of $^2P_{3/2}$ and $^2P_{1/2}$ is through spin-orbit relaxation. The spin-orbit relaxation can be speed up by adding spin-mixing gas. The excited population decays to ground level of $^2S_{1/2}$ through three ways. They are stimulated emission, spontaneous emission and quenching. Compared with the stimulated and spontaneous emission rates, quenching rate is much smaller. Thus, quenching can be negligible in the model. Population densities on the levels of $^2S_{1/2}$, $^2P_{1/2}$ and $^2P_{3/2}$ are denoted as $n_1$, $n_2$ and $n_3$, respectively. Here, the population densities are average values along the longitudinal axis of cell, $n_i=\int n_i(z)\mathrm{d}z/l$ ($i=1$, 2 and 3). $l$ is the length of vapor cell and $z$ is the longitudinal axis of cell. The total density of alkali atoms in the cell is denoted as $n_0$.

The rate equations of alkali vapor lasers can be expressed as

$$\begin{cases} \frac{dn_1}{dt}=-\left(n_1-\frac{1}{2}n_3\right)\sigma_{D2}\frac{I_{p-cav}}{h\nu_{D2}}+(n_2-n_1)\sigma_{D1}\frac{I_{L-cav}}{h\nu_{D1}}+n_3A_{31}+n_2A_{21} \\ \frac{dn_2}{dt}=-(n_2-n_1)\sigma_{D1}\frac{I_{L-cav}}{h\nu_{D1}}+\gamma_{32}\left\{n_3-2n_2\exp\left[-\frac{\Delta E}{k_BT}\right]\right\}-n_2A_{21} \\ \frac{dn_3}{dt}=\left(n_1-\frac{1}{2}n_3\right)\sigma_{D2}\frac{I_{p-cav}}{h\nu_{D2}}-\gamma_{32}\left\{n_3-2n_2\exp\left[-\frac{\Delta E}{k_BT}\right]\right\}-n_3A_{31} \\ n_1+n_2+n_3=n_0 \end{cases} \quad (1)$$

here, $\sigma_{D2}$ and $\sigma_{D1}$ are the absorption and emission cross sections at each line center, respectively. $\nu_{D1}$ and $\nu_{D2}$ are the center frequencies of D1 and D2 transitions, respectively. $A_{21}$ and $A_{31}$ are the spontaneous emission rates of population on the levels of $^2P_{1/2}$ and $^2P_{3/2}$, respectively. $\Delta E$ is the energy defect between fine structure levels of $^2P_{1/2}$ and $^2P_{3/2}$. $\gamma_{32}$ is the spin–orbit relaxation rate (or fine structure mixing rate). $h$ is the Planck constant and $k_B$ is the Boltzmann constant. $T$ is the temperature of alkali vapor. Here, the vapor temperature distribution is assumed to be uniform and equals to the cell wall temperature $T_{wall}$. This assumption is made for easy modeling and analysis. Actually, the temperature distribution is non-uniform in high power DPAL [15]. However, this problem can be mitigated in flowing-gas DPAL [16–18]. $I_{L\text{-}cav}$ and $I_{p\text{-}cav}$ are the laser and pump intensities within the cell, respectively. $I_{p\text{-}cav}$ is expressed as

$$I_{p-cav}=\int_{-\infty}^{+\infty} g_{D2}(\nu,\nu_{D2})I_{p-cav}(\nu,\nu_p)\,d\nu \quad (2)$$

here, $g_{D2}(\nu,\nu_{D2})$ is the normalized Lorentzian line shape of D2 transition, $g_{D2}(\nu,\nu_{D2})=1/\{1+[(\nu-\nu_{D2})/(\Delta\nu_{D2}/2)]^2\}$. $\Delta\nu_{D2}$ is the full-width half maximum (FWHM) spectrum width of D2 transition broadened by helium. $I_{p\text{-}cav}(\nu,\nu_p)$ is the spectrally resolved pump intensity within the cell. $\nu_p$ is the center frequency of pump light. In double-pass pump configuration, $I_{p\text{-}cav}(\nu,\nu_p)$ is given by

$$I_{p-cav}(\nu,\nu_p)=\frac{I_{pin}(\nu,\nu_p)}{\alpha(\nu,\nu_{D2})l}t_p\{1-\exp[-\alpha(\nu,\nu_{D2})l]\}\left\{1+r_pt_p^2\exp[-\alpha(\nu,\nu_{D2})l]\right\} \quad (3)$$

here, $I_{pin}(\nu,\nu_p)$ is the spectrally resolved input pump intensity, $I_{pin}(\nu,\nu_p)=I_{pin}g_p(\nu,\nu_p)$. $I_{pin}$ is the total input pump intensity integrated on the whole spectrum. $g_p(\nu,\nu_p)$ is the spectral distribution of pump light. $\alpha(\nu,\nu_{D2})$ is the spectrally resolved absorption coefficient, $\alpha(\nu,\nu_{D2})=(n_1-n_3/2)\sigma_{D2}g_{D2}(\nu,\nu_{D2})$. $t_p$ and $r_p$ are the transmission of cell window and reflectivity of output mirror at pump wavelength, respectively.

If the pump light is monochromatic and its frequency equals to the center frequency of D2 transition, $g_p(\nu,\nu_p)=\delta(\nu,\nu_{D2})$, $I_{p\text{-}cav}$ will be equivalent to the longitudinally averaged two-way pump intensity in Hager's model [19]. In this model, the pump light is supposed to be a Gauss profile with a FWHM spectrum width of $\Delta\nu_p$ in Eq. (4).

$$g_p(\nu,\nu_p)=\frac{2}{\Delta\nu_p}\sqrt{\frac{\ln 2}{\pi}}\exp\left\{-\ln 2\left[\frac{\nu-\nu_p}{\Delta\nu_p/2}\right]^2\right\} \quad (4)$$

Assuming that the first three derivatives of Eq. (1) equal zero, the steady state solution of hydrocarbon free DPAL will be found. By using the experiment condition data of hydrocarbon free K laser in Ref. [14], the model is tested. Simulated results for the slope efficiency and peak laser efficiency are about 66% and 62%, respectively. Experimental values of these two efficiencies are 64% and 57%, respectively. The accordant results indicate that this model is a reliable method for analyzing the laser performance of hydrocarbon free DPALs.

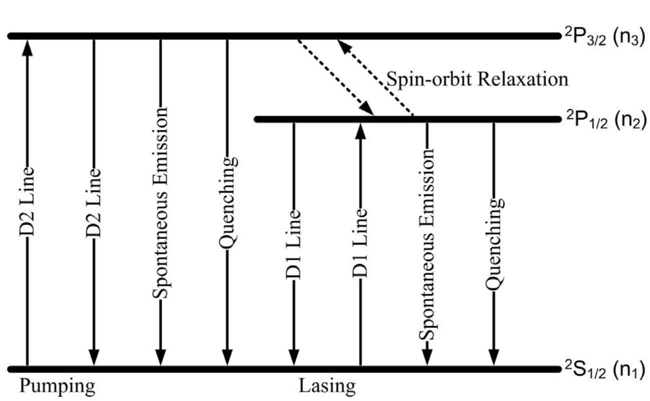


**Fig. 1.** Energy levels and main kinetic processes of alkali vapor laser.

## 3. Results and Discussions

### 3.1. Optimal operation of hydrocarbon free DPALs

Except output laser energy, the pump laser absorbed by alkali vapor is all converted into thermal energy, scattering energy and fluorescence energy. In the energy balance Eq. (5), the terms of $P_{abs}$ and $P_{laser}$ denote the pump power absorbed by alkali vapor and laser power, respectively. $P_{ther}$ is the thermal power, and it relates to the energy defect $\Delta E$ and results in waste heat. $P_{scat}$ is the scattering power, which is resulted from the non-perfect window transmission. $P_{fluo}$ represents the fluorescence power due to spontaneous emission. Eq. (6) describes the conversion process in the form of efficiencies, which are absorption efficiency, laser efficiency, thermal efficiency, scattering efficiency and fluorescence efficiency.

Here, laser efficiency denotes the optical-to-optical efficiency.

$$P_{abs} = P_{laser} + P_{ther} + P_{scat} + P_{fluo} \tag{5}$$

$$\eta_{abs} = \eta_{laser} + \eta_{ther} + \eta_{scat} + \eta_{fluo} \tag{6}$$

Based on the model described in part 2, the parameters of helium pressure, temperature and output mirror reflectivity are optimized to achieve the highest laser efficiencies of hydrocarbon free DPALs. Here, naturally-occurring helium ($^4$He) is injected into the vapor cell to collisionally broaden the D2 line and enhance the mixing of alkali fine structure levels. The data of broadening rates and mixing cross sections are listed in Table 1. Since the mixing cross section of Cs-$^4$He is so small that the hydrocarbon free Cs laser is not simulated. The pump intensity for hydrocarbon free Rb and K lasers is set to be 10 kW/cm$^2$. It should be noted that the photoionization and Penning ionization will strongly degrade the laser performance by reducing the alkali atom density at high pump intensity [18,25,26]. However, these ionization processes are ignored in the model. If a flowing-gas scheme is utilized, the reduced alkali atoms can be replenished. The pump beam is supposed to be cylindrical with a radius of 400 μm. The spectral distribution of pump light is Gaussian profile and centered on each alkali D2 line. The FWHM spectrum width of the pump light is 15 GHz. The narrow pump spectrum width is to avoid parasitic excitation. If the pump spectrum is too wide, the red wing of pump light may excite D1 transition (770.1 nm ) of K atom, and the blue wing of pump light may excite $^5P_{3/2} \rightarrow {}^5D_{5/2}$ transition (776 nm) of Rb atom. The length of vapor cell is 5 cm. The transmissions of cell window at both the pump and laser wavelengths are 97.5%. The output mirror reflectivity $r_p$ at pump wavelength is 100%. It means that the pump light can be totally reflected back into the cell by output mirror after one pass. The alkali vapor will be highly bleached in this double-pass pump configuration.

In Fig. 2, the laser efficiency and thermal efficiency of the two lasers at different temperature are plotted. For explicit display, the thermal efficiency is 10 times the actual value. Fig. 3 gives the corresponding absorption efficiency, scattering efficiency and fluorescence efficiency. The vertical dot lines in Figs. 2 and 3 denote the optimal operation states of Rb and K lasers. In this state, the system is operated at the highest laser efficiency.

It can be seen that the laser efficiencies of Rb and K lasers are increased to the maximum and then begin to decrease with the increase of temperature. The temperature corresponding to the maximum laser efficiency is the optimal operation temperature. Increasing temperature leads to increasing alkali atom density. This will lead to two issues: (1) more pump power will be absorbed, which will benefit laser extracting in certain extent; and (2) more fluorescence power will be generated exponentially, which means more pump power will be wasted. If temperature increases in the region below the optimal operation temperature, the absorbed pump power increases linearly. In this case, the former issue is dominant and more pump energy is converted into laser energy. Once the temperature rises to the optimal operation temperature, the absorbed pump power begins to be saturated and laser efficiency reaches the maximum value. If temperature is beyond the optimal operation temperature, the latter issue will be dominant. In this case, almost 100% of the pump power is absorbed. But the fluorescence power increases rapidly, which leads to the decrease of laser efficiency.

It is also shown that the thermal efficiency and scattering efficiency have similar temperature dependence with laser efficiency. Moreover, thermal efficiency also reaches its maximum value at the optimal operation temperature as laser efficiency. It is due to that both of the heat generating and laser extracting are deeply related to the fine structure mixing rate.

### 3.2. Performance comparison between hydrocarbon free DPALs

As shown in Fig. 2, it can be concluded that both the two lasers can be operated in buffer gas system of pure $^4$He gas efficiently. However, unlike the laser performance in hydrocarbon buffer gas system, a better capability is presented in the hydrocarbon free K laser instead of hydrocarbon free Rb laser. For a simple

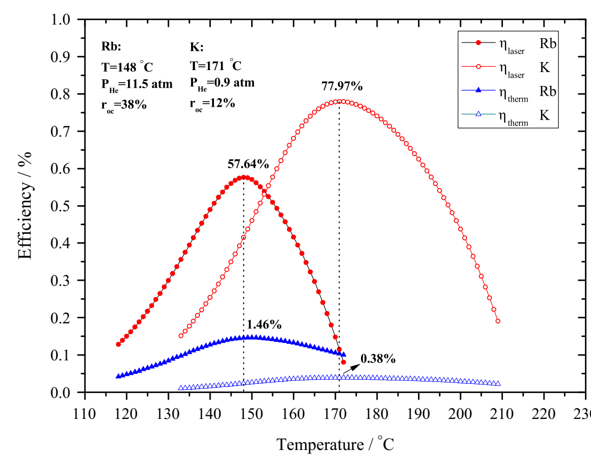


**Fig. 2.** Laser efficiency (○) and thermal efficiency (▵, 10 times the actual value) of hydrocarbon free Rb (solid) laser and K (hollow) laser at different temperatures.

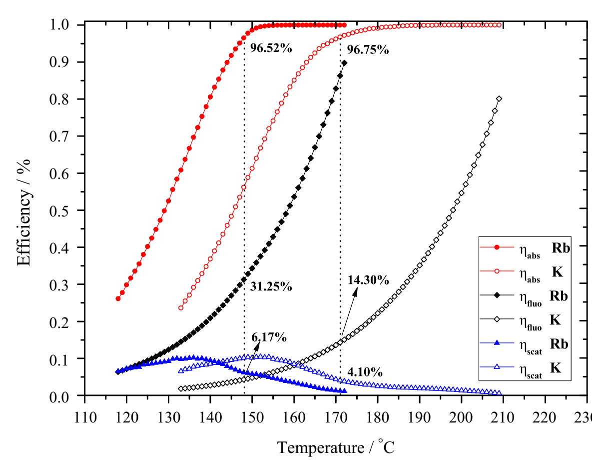


**Fig. 3.** Absorption efficiency (○), fluorescence efficiency (◇) and scattering efficiency (▵) of hydrocarbon free Rb laser (solid) and K laser (hollow) at different temperatures.

**Table 1**
Broadening rates and mixing cross sections of K, Rb and Cs ($^4$He in cell).

| Alkali species | K | Refs. | Rb | Refs. | Cs | Refs. |
|---|---|---|---|---|---|---|
| Broadening rate on D1 line/GHz amg$^{-1}$ | 14.1 | [20] | 18.0 | [22] | 19.3 | [24] |
| Broadening rate on D2 line/GHz amg$^{-1}$ | 19.9 | [20] | 18.1 | [22] | 21.5 | [24] |
| Mixing cross section/cm$^2$ | $1.78 \times 10^{-15}$ | [21] | $1.03 \times 10^{-17}$ | [23] | $3.9 \times 10^{-20}$ | [11] |

comparison, the optimal operation conditions and laser parameters in pure $^4$He gas are listed in Table 2.

Firstly, at each optimal operation temperature, hydrocarbon free K laser has less fluorescence radiation than hydrocarbon free Rb laser (as shown in Fig. 3). Compared with 31.25% of Rb laser, the fluorescence efficiency of K laser is 14.30%. In the mode volume $V_{\mathrm{mode}}$, fluorescence power is mainly influenced by the amount of excited population ($n_2$ and $n_3$) and spontaneous emission rates ($A_{21}$ and $A_{31}$). The fluorescence power is expressed as $P_{\mathrm{fluo}} = h(\nu_{D1} n_2 A_{21} + \nu_{D2} n_3 A_{31}) V_{\mathrm{mode}}$. As shown in Table 2, the spontaneous emission rates of excited K and Rb atoms are very close, so the fluorescence power is mainly influenced by the amount of excited population. The excited population of K atoms is $2.92 \times 10^{13}\ \mathrm{cm}^{-3}$ in the comparison with $6.63 \times 10^{13}\ \mathrm{cm}^{-3}$ of Rb atoms. Therefore, less energy is wasted on the fluorescence in hydrocarbon free K laser. On the other hand, the less fluorescence radiation of hydrocarbon K laser can be explained through the view of transition rate. The stimulated emission rate is about 16 times the spontaneous emission rate in K laser, but the ratio of Rb laser is 5. The stimulated emission of K laser is much more dominant than that of Rb laser. Thus, the fluorescence radiation can be suppressed better in hydrocarbon free K laser.

Secondly, the helium pressure of hydrocarbon free K laser is much lower than that of hydrocarbon free Rb laser. For the quite large mixing cross section of K-$^4$He, the helium pressure of K laser is 0.9 atm compared with 11.5 atm of Rb laser. In hydrocarbon free Rb laser, much more helium atoms are needed to achieve fast enough fine structure mixing rate. However, the same fine structure mixing rate can be achieved with less than 1 atm of mixed gas of $^4$He-$C_2H_6$ in hydrocarbon Rb laser. The high helium pressure of hydrocarbon free Rb laser will not only make the vapor cell fabrication very difficult, but also induce the degradation of laser performance.

In DPAL, the stimulated absorption and emission cross sections are inversely proportional to the spectrum width of D2 or D1 transition, which is broadened by helium gas. Thus, the cross sections will be decreased with the increase of helium pressure. As shown in Table 2, the cross-section magnitude of Rb laser is $10^{-14}\ \mathrm{cm}^2$ compared with $10^{-13}\ \mathrm{cm}^2$ of K laser. With the sharp decrease of cross section, laser gain and threshold pump power will be influenced.

1) In hydrocarbon buffer gas system, the laser gain of Rb laser is larger than that of K laser due to the larger inverted population of Rb laser [7], $g = \Delta n_{21} \sigma_{D1}$. But in hydrocarbon free buffer gas system, the dominant factor is the emission cross section. As shown in Table 2, the inverted population of Rb laser is $3.58 \times 10^{12}\ \mathrm{cm}^{-3}$ and occupies 3.92% of the total Rb atoms, compared with $4.47 \times 10^{11}\ \mathrm{cm}^{-3}$ and 1.14% of K laser. Due to the much smaller emission cross section of Rb atoms, the laser gain of Rb laser is only $0.11\ \mathrm{cm}^{-1}$ which is half of the laser gain of K laser. The smaller laser gain of hydrocarbon free Rb laser can also be explained by its larger output mirror reflectivity $r_{oc}$. For evident comparison, the dependences of output power on output mirror reflectivity of the two lasers are plotted in Fig. 4. The vertical dot lines denote the optimal operation states. Here, the output power is calculated by supposing that both the two lasers have perfect mode matching degrees, $\eta_{\mathrm{mode}} = (r_L/r_P)^2 = 1$.
2) In DPALs, the threshold pump power has a dependence not only on the energy defect $\Delta E$ but also on the saturated pump intensity $I_{sp}$, $I_{sp} = 2A_{31} h\nu_p / \sigma_{D2}$. In hydrocarbon buffer gas system, a larger threshold pump power is presented in K laser due to the smaller energy defect of K atom. However, absorption cross section is also a dominant factor in hydrocarbon free buffer gas system. Because of the small absorption cross section of Rb atom, the saturated pump intensity of Rb laser is quite large as $350.7\ \mathrm{W/cm}^2$. But the saturated pump intensity of K laser is $28.1\ \mathrm{W/cm}^2$. This will cause a higher threshold pump power of Rb laser.

The dependences of output power on input power of these two lasers are plotted in Fig. 5. The vertical dot lines denote the optimal operation states and the hatched parts denote the

**Table 2**
Operation conditions and laser parameters in optimal states.

| Parameter Description | K laser ($^4$He) | Rb laser ($^4$He) | Rb laser ($^3$He) |
|---|---|---|---|
| **Optimal operation condition** | | | |
| Operation temperature $T$ (°C) | 171 | 148 | 145 |
| Helium pressure $P_{He}$(atm) | 0.9 | 11.5 | 8 |
| Reflectivity of output mirror $r_{oc}$ (%) | 12 | 38 | 34 |
| **Alkali spectral parameters** | | | |
| Bandwidth of D1 transition $\Delta\nu_{D1}$ (GHz) | 11.4 | 193.9 | 140.1 |
| Stimulated emission cross section $\sigma_{D1}$ (cm$^2$) | $4.97 \times 10^{-13}$ | $2.98 \times 10^{-14}$ | $4.13 \times 10^{-14}$ |
| Bandwidth of D2 transition $\Delta\nu_{D2}$ (GHz) | 16.16 | 212.2 | 169.0 |
| Stimulated absorption cross section $\sigma_{D2}$ (cm$^2$) | $6.99 \times 10^{-13}$ | $5.54 \times 10^{-14}$ | $6.95 \times 10^{-14}$ |
| **Alkali population parameters** | | | |
| $^2S_{1/2}$ population $n_1$ (cm$^{-3}$) | $1.01 \times 10^{13}$ | $2.50 \times 10^{13}$ | $2.16 \times 10^{13}$ |
| $^2P_{1/2}$ population $n_2$ (cm$^{-3}$) | $1.06 \times 10^{13}$ | $2.86 \times 10^{13}$ | $2.44 \times 10^{13}$ |
| $^2P_{3/2}$ population $n_3$ (cm$^{-3}$) | $1.86 \times 10^{13}$ | $3.77 \times 10^{13}$ | $3.25 \times 10^{13}$ |
| **Transition rate parameters** | | | |
| D1 spontaneous emission rate $A_{21}$ (s$^{-1}$) | $3.79 \times 10^7$ | $3.61 \times 10^7$ | $3.61 \times 10^7$ |
| D2 spontaneous emission rate $A_{31}$ (s$^{-1}$) | $3.79 \times 10^7$ | $3.81 \times 10^7$ | $3.81 \times 10^7$ |
| Fine structure mixing rate $\gamma_{32}$ (s$^{-1}$) | $6.98 \times 10^9$ | $4.90 \times 10^8$ | $5.85 \times 10^8$ |
| Stimulated emission rate $W_{21}$ (s$^{-1}$) | $6.00 \times 10^8$ | $1.79 \times 10^8$ | $2.26 \times 10^8$ |
| Stimulated absorption rate $W_{13}$ (s$^{-1}$) | $7.36 \times 10^8$ | $3.03 \times 10^8$ | $3.55 \times 10^8$ |
| **Efficiency** | | | |
| Absorption efficiency $\eta_{abs}$ (%) | 96.75 | 96.52 | 97.53 |
| Laser efficiency $\eta_{laser}$ (%) | 77.97 | 57.64 | 63.11 |
| Thermal efficiency $\eta_{ther}$ (%) | 0.38 | 1.45 | 1.52 |
| Scattering efficiency $\eta_{scat}$ (%) | 4.10 | 6.17 | 6.09 |
| Fluorescence efficiency $\eta_{fluo}$ (%) | 14.30 | 31.25 | 26.81 |

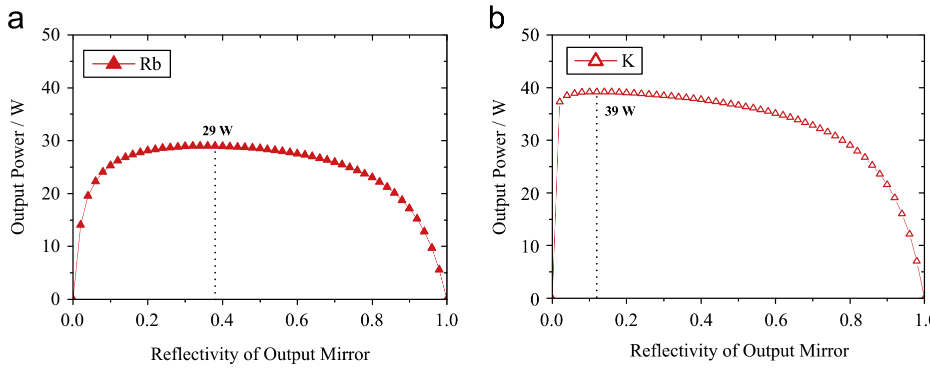


**Fig. 4.** Dependence of output laser power on the output mirror reflectivity. (a) Rb laser ($T$=148 °C) and (b) K laser ($T$=171 °C).

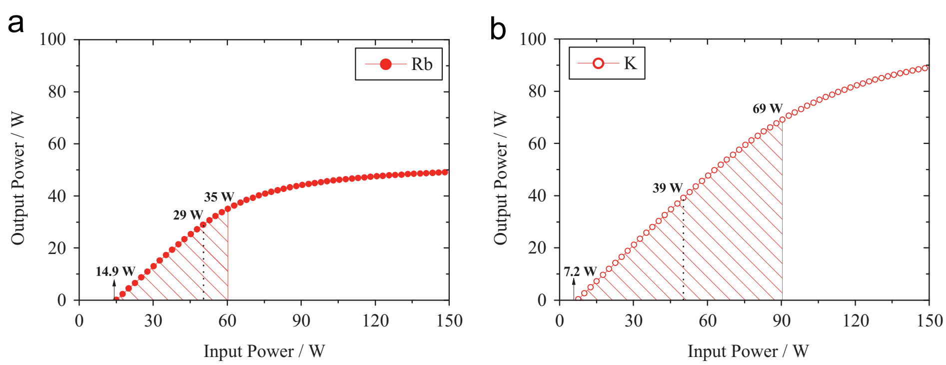


**Fig. 5.** Dependence of output power on input power (a) Rb laser ($T$=148 °C, $r_{oc}$=38%); (b) K laser ($T$=171 °C, $r_{oc}$=12%).

region in which the output power increases linearly with the increase of input power. It is clear that the threshold pump power of Rb laser is as large as 14.9 W, but that power of K laser is only 7.2 W. In hydrocarbon free Rb laser, more energy is used to establish the oscillation of laser mode. Besides, it is also obvious that the linear operation region of K laser is more extensive than that of Rb laser. This is due to the larger fine structure mixing rate of K laser.

Thirdly, to reduce the helium pressure, $^4$He is replaced by isotopically enriched $^3$He. Compared with $^4$He, $^3$He has lower mass and hence it can offer higher thermally relative velocity between Rb atoms and $^3$He atoms, $v_r=[3k_BT(1/m_{He}+1/m_{Rb})]^{1/2}$. The higher velocity will contribute to enhancing the mixing rate, $\gamma_{32}=n_{He}\sigma_{mix}v_r$. Here, $n_{He}$ is number density of He atoms, $\sigma_{mix}$ is the mixing cross section. Besides, the broadening rate of $^3$He on D2 transition of Rb is as large as 20.8 GHz amg$^{-1}$ compared with 18.1 GHz amg$^{-1}$ of $^4$He [16]. Therefore by using $^3$He as buffer gas, the pressure can be reduced and hence laser performance can be improved. The optimal operation conditions and laser parameters of Rb laser in pure $^3$He gas are also listed in Table 2. It is clear that the laser efficiency is improved and the fluorescence radiation is suppressed. Experiments also showed the advantages of using $^3$He as buffer gas. Under the same $^4$He pressure of 2.7 atm in Ref. [12], the output power is as high as 350 mW with an optical-to-optical efficiency of 21% by using $^3$He [27].

Concluded from above performance comparisons, hydrocarbon free K laser has some advantages as follow: (1) less fluorescence; (2) higher laser gain; and (3) lower threshold pump power. Because of these merits, higher laser efficiency can be obtained in hydrocarbon free K laser. Besides, performance of hydrocarbon free Rb laser can be improved to some extent in pure $^3$He gas.

## 4. Conclusions

Based on the end-pumped three-level laser rate-equation model, the laser characteristics of hydrocarbon free Rb laser and K laser are simulated and analyzed. In optimal operation states, the $^4$He pressure is more than 11 atm in Rb laser and less than 1 atm in K laser. Results show that the laser efficiency reaches the highest value when the absorbed pump power begins to be saturated. However, the Rb laser capability is degenerated because of the high $^4$He pressure. On the contrary, a better performance is presented in K laser, such as lower pump threshold, higher laser gain and higher optical-to-optical efficiency. Moreover, the fluorescence is suppressed in K laser and it can be operated in a more extensive linear region with extremely low waste heat. If the bandwidth of pump source is small enough to avoid pump wing parasitic excitation effect, the merits of hydrocarbon free K laser will make itself an efficient laser system.

## Acknowledgment

This work was supported by the National Natural Science Foundation of China under Grant no. 61308050 and Fundamental Research Project of Chinese State Key Laboratory of Laser Interaction with Matter under Grant no. SKLLIM 1210-01.

## References

[1] Krupke WF, Beach RJ, Kanz VK, Payne SA. Resonance transition 795-nm rubidium laser. Opt Lett 2003;28:2336–8.

[2] Ehrenreich T, Zhdanov B, Takekoshi T, Phipps SP, Knize RJ. Diode pumped caesium laser. Electron Lett 2005;41:47–8.
[3] Bogachev AV, Garanin SG, Dudov AM, Yeroshenko VA, Kulikov SM, Mikaelian GT, Panarin VA, Pautov VO, Rus AV, Sukharev SA. Diode-pumped caesium vapour laser with closed-cycle laser-active medium circulation. Quantum Electron 2012;42:95–8.
[4] Zweiback J, Komashko A, Krupke WF. Alkali vapor lasers. Proc SPIE 2010;7581:75810G.
[5] Zhdanov BV, Shaffer MK, Knize RJ. Demonstration of a diode pumped continuous wave Potassium laser. Proceedings of the SPIE 2011;7915:791506.
[6] Zweiback J, Krupke B, Komashko A. Diode pumped alkali vapor lasers for high power applications. Proceedings of the SPIE 2008;6874:68740G.
[7] Krupke WF. Diode pumped alkali lasers (DPALs)—a review. Prog Quant Electron 2012;36:4–28.
[8] Wang H, Yang Z, Hua W, Xu X, Lu Q. Choice of alkali element for DPAL scaling, a numerical study. Opt Commun 2013;296:101–5.
[9] Yang Z, Wang H, Lu Q, Liu L, Li Y, Hua W, Xu X, Chen J. Theoretical model and novel numerical approach of a broadband optically pumped three-level alkali vapour laser. J Phys B: At Mol Opt Phys 2011;44:085401.
[10] Zhdanov BV, Knize RJ. Diode-pumped 10 W continuous wave cesium laser. Opt Lett 2007;32:2167–9.
[11] Czajkowski M, Mcgillis DA, Krause L. Sensitized fluorescence in vapors of alkali metals V. Energy transfer in collisions between cesium and inert gas atoms. Can J Phys 1966;44:91–103.
[12] Wu Sheldon SQ, Soules TF, Page RH, Mitchell SC, Kanz VK, Beach RJ. Hydrocarbon-free resonance transition 795-nm rubidium laser. Opt Lett 2007;32:2423–5.
[13] Zweiback J, Krupke WF. 28 W average power hydrocarbon-free rubidium diode pumped alkali laser. Opt Exp 2010;18:1444–9.
[14] Zweiback J, Hager G, Krupke WF. High efficiency hydrocarbon-free resonance transition potassium laser. Opt Commun 2009;282:1871–3.
[15] Zhu Q, Pan B, Chen L, Wang Y, Zhang X. Analysis of temperature distributions in diode-pumped alkali vapor lasers. Opt Commun 2010;283:2406–10.
[16] Yang Z, Wang H, Lu Q, Li Y, Hua W, Xu X, Chen J. Modeling, numerical approach, and power scaling of alkali vapor lasers in side-pumped configuration with flowing medium. J Opt Soc Am B 2011;28:1353–64.
[17] Barmashenko BD, Rosenwaks S. Modeling of flowing gas diode pumped alkali lasers: dependence of the operation on the gas velocity and on the nature of the buffer gas. Opt Lett 2012;37:3615–7.
[18] Barmashenko BD, Rosenwaks S. Detailed analysis of kinetic and fluid dynamic processes in diode-pumped alkali lasers. J Opt Soc Am B 2013;30:1118–26.
[19] Hager G, Perram. G. A three-level analytic model for alkali metal vapor lasers: part I narrowband optical pumping. Appl Phys B 2010;101:45–56.
[20] Kantor PY, Penkin NP, Shaabnov LN. Broadening of the KI 769.9 and 766.5 nm lines by inert gases. Opt Spectrosc 1985;59:151–5.
[21] Ciury J, Krause L. $4^2P_{1/2}$-$4^2P_{3/2}$ mixing in potassium induced in collisions with noble gas atoms. J Quant Spectrosc Radiat Transf 1982;28:457–61.
[22] Romalis MV, Miron E, Gates GD. Pressure broadening of Rb $D_1$ and $D_2$ lines by $^3$He, $^4$He, $N_2$, and Xe: Line cores and near wings. Phys Rev A 1997;56:4569–78.
[23] Pitre B, Rae AGA, Krause L. Sensitized fluorescence in vapors of alkali metals. VI. Energy transfer in collisions between rubidium and inert gas atoms. Can J Phys 1966;44:731–7.
[24] Andalkar A, Warrington RB. High-resolution measurement of the pressure broadening and shift of the Cs D1 and D2 lines by $N_2$ and He buffer gases. Phys Rev A 2002;65:032708.
[25] Barmashenko BD, Rosenwaks S, Heaven MC. Static diode pumped alkali lasers: Model calculations of the effects of heating, ionization, high electronic excitation and chemical reactions. Opt Commun 2013;292:123–5.
[26] Knize RJ, Zhdanov BV, Shaffer. MK. Photoionization in alkali lasers. Opt Exp 2011;19:7894–902.
[27] Wu Sheldon SQ, Soules TF, Page RH, Mitchell SC, Kanz VK, Beach RJ. Resonance transition 795-nm rubidium laser using $^3$He buffer gas. Opt Commun 2008;281:1222–5.